



Shale Lithofacies and Its Effect on Reservoir Formation in Lower Permian Alkaline Lacustrine Fengcheng Formation, Junggar Basin, NW China

Yong Tang¹, Wenjun He¹, Menglin Zheng¹, Qiusheng Chang¹, Zhijun Jin², Jiao Li^{2,3} and Yuanyuan Zhang^{2,3*}

¹PetroChina Xinjiang Oilfield Company, Karamay, China, ²Institute of Energy, Peking University, Beijing, China, ³School of Earth and Space Sciences, Peking University, Beijing, China

OPEN ACCESS

Edited by:

Dongdong Liu,
China University of Petroleum, Beijing,
China

Reviewed by:

Xianglu Tang,
China University of Petroleum, Beijing,
China
Lei Chen,
China University of Petroleum,
Huadong, China

*Correspondence:

Yuanyuan Zhang
yy-zhang@pku.edu.cn

Specialty section:

This article was submitted to
Economic Geology,
a section of the journal
Frontiers in Earth Science

Received: 28 April 2022

Accepted: 05 May 2022

Published: 05 August 2022

Citation:

Tang Y, He W, Zheng M, Chang Q, Jin Z, Li J and Zhang Y (2022) Shale Lithofacies and Its Effect on Reservoir Formation in Lower Permian Alkaline Lacustrine Fengcheng Formation, Junggar Basin, NW China. *Front. Earth Sci.* 10:930890. doi: 10.3389/feart.2022.930890

Lower Permian Fengcheng Formation is considered to be a high-quality alkaline lacustrine shale oil resource in the Junggar Basin, NW China. Based on core and thin section observation, X-ray diffraction, scanning electron microscope, low-pressure N₂ adsorption, and high-pressure mercury intrusion porosimetry, different shale lithofacies, and pore structures were examined. According to the mineral composition, shales in well My 1 are divided into five types: dolomitic mudstone, calcareous mudstone, siliceous mudstone, tuffaceous mudstone, and argillaceous mudstone, each of which shows its pore structure distribution. Intragranular pores, inter-crystalline pores associated with clays and pyrites, dissolution pores, and microfractures were commonly observed. There are three segments of pore structures including <50 nm, 50 nm–4 μm, and >4 μm. Clay minerals mainly contribute to mesopores, especially in argillaceous mudstones. The dissolution of carbonate minerals and feldspars is significant for macropores predominantly in dolomitic mudstones and tuffaceous mudstones, respectively. Micron-scale microfractures associated with laminae dominate in dolomitic mudstones. Therefore, the dolomitic mudstones, especially with lamination, and tuffaceous mudstones are proposed to be favored shale lithofacies with great exploration potential in the Mahu Sag.

Keywords: shale lithofacies, pore structure, fengcheng formation, alkaline lacustrine, reservoir formation

1 INTRODUCTION

Lacustrine shale oil in China has proven to show tremendous potential for exploration and development, which are strategically crucial for increasing the nation's hydrocarbon reserves and production (Jin et al., 2021). Compared with marine oil shales, lacustrine shales in China are characterized by strong heterogeneity with rapid facies changes, complex lithologies, and diverse reservoir-seal assemblages (Li et al., 2019). To date, exploration for shale oil is concentrated in saline or brackish lacustrine basins (e.g., the Paleogene Shahejie Formation in the Bohai Bay Basin, the Paleogene Qianjiang Formation in the Jiangnan Basin, and the Songliao Basin) (e.g., Gao et al., 2018; Chen et al., 2019; Xue et al., 2020; Hu et al., 2022).

Alkaline lacustrine deposits are deposited in extremely salinized lakes that develop high-quality oil shales with great hydrocarbon potential. The shale of the Eocene Green River Formation in the United States is a well-known example. The Fengcheng Formation in the Mahu Sag, in the Junggar Basin in northwestern China, boasts ancient alkaline lacustrine deposits with integrated sources and

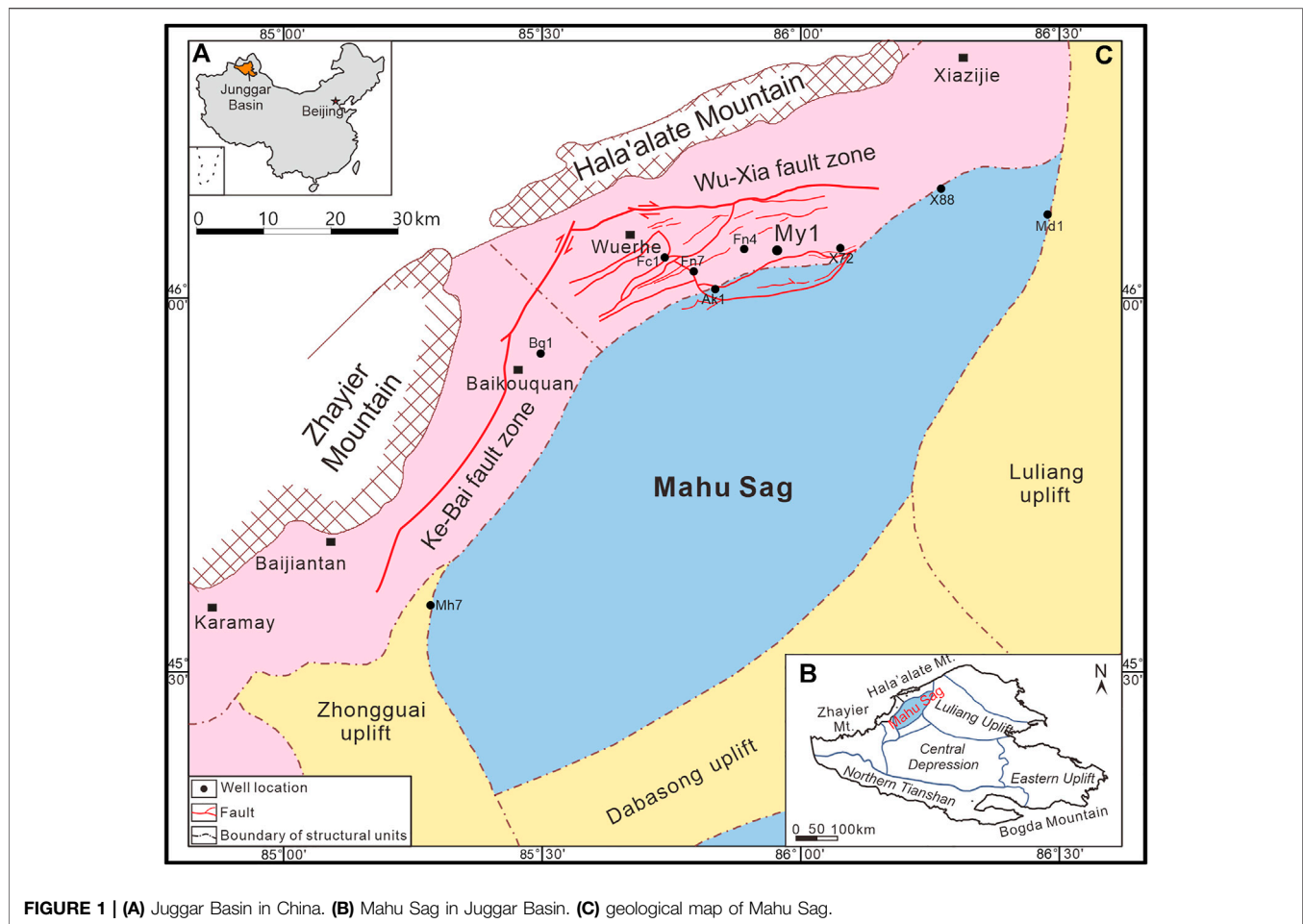


FIGURE 1 | (A) Junggar Basin in China. (B) Mahu Sag in Junggar Basin. (C) geological map of Mahu Sag.

reservoirs. These are considered to represent a new type of alkaline lacustrine shale oil reservoir and the formation has huge shale oil potential (Zhi et al., 2019; Tang et al., 2021).

Lacustrine shales with varied compositions have complex origins. Add to this the discrepancies in depositional environments and depositional processes in lacustrine basins and the result is complex, fine-grained, sedimentary rock facies with correspondingly complex pore structures (Zou et al., 2013; Barth-Naftilan et al., 2015; Wang et al., 2020). Fine description and division of alkaline-lacustrine fine-grained sedimentary rocks is therefore a vital prerequisite for the study of reservoir types and quantitative characterization of alkaline lacustrine shale oil reservoirs.

This study examines the fine-grained sedimentary rocks of the Fengcheng Formation in the Early Permian alkaline lacustrine deposits in the Mahu Sag. The alkaline-lacustrine shale facies are classified using core and thin section observations, scanning electron microscope (SEM), and imaging analysis. Pore size distributions and pore structures are quantitatively analyzed with a combination of low-pressure nitrogen adsorption and high-pressure mercury injection. The objective of this study is eventually to identify favorable lithofacies in the formation and determine the controlling factors.

2 GEOLOGICAL SETTING

The Junggar Basin is one of the most important petroliferous superimposed basins in Northwest China (Ma et al., 2008; He et al., 2018) (Figure 1). This study focuses on the Mahu Sag, the most crucial hydrocarbon-generating sag in the basin (Zhi et al., 2021). The Mahu Sag is near the basin's northwestern margin, with the Zaire and Hala'ate mountains to the northwest and the Zhongguai, Dabasang, and Luliang uplift to the southeast. It evolved with a major NE-SW trending tectonic depression adjacent to the Karamay-Baikouquan (Ke-Bai) and Wuerhe-Xiazijie (Wu-Xia) fault zones (Figure 1C).

The Lower Permian Fengcheng Formation in the Mahu Sag is considered to be the oldest alkaline lacustrine deposit and is rich in shale oil with source-reservoir integration (Cao et al., 2015, 2020; Tang et al., 2021; Wang et al., 2021). The Fengcheng Formation is also the primary source of hundreds-of-miles oil provinces across the northwestern part of the Junggar Basin (Cao et al., 2015; Li et al., 2020). The success of well My1 confirms the enormous exploration potential of the formation and, generally, the potential of shale oil in alkaline lacustrine settings (Tang et al., 2021).

The Fengcheng Formation varies in thickness from 800 to 1800 m, thinning from west to east. It is divided into a lower

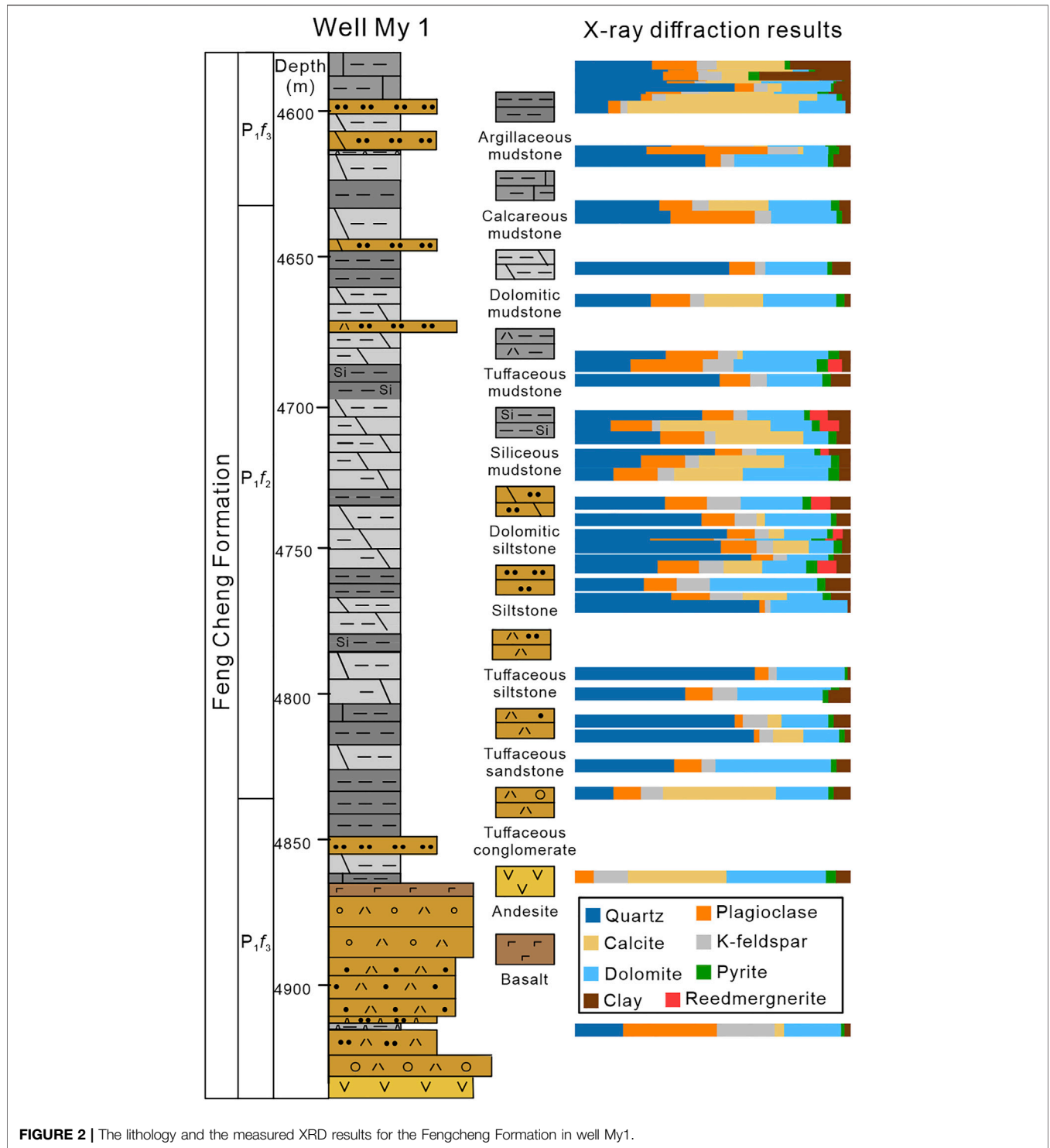


FIGURE 2 | The lithology and the measured XRD results for the Fengcheng Formation in well My1.

member (P_1f_1), a middle member (P_1f_2), and an upper member (P_1f_3). P_1f_1 is mainly composed of gray or dark gray mudstone and tuffaceous mudstone with interbedded dolomitic sandstone, dolomite, tuffaceous dolomite, argillaceous dolomite, and tuff, indicating relatively intense volcanic activity. P_1f_2 contains dolomitic sandstone and mudstone with interbedded

argillaceous dolomite and a wide variety of alkaline minerals. P_1f_3 is predominantly mudstone intercalated with dolomitic mudstone in the lower interval and terrigenous clastic sedimentary rocks in the upper interval.

Well My1 was drilled in the northeastern margin of the Mahu Sag (Figure 1C) and obtained a relatively complete core section of

the Fengcheng Formation (4,580–4,930 m) (**Figure 2**). The thickness of P_{1f_1} in the core section was more than 100 m, and that of P_{1f_2} about 200 m. The core section did not reach the top of P_{1f_3} . Nevertheless, it facilitates the study of the lithofacies and pore development of the alkaline lacustrine shale in the formation.

3 SAMPLES AND METHODS

Core observation and description for well My1 were carried out using 99 shale samples taken at depths of 4,614 m–4,939 m (**Figure 2**). Petrography and pore types were determined using both optical and scanning electron microscope (SEM) with energy-dispersive X-ray spectroscopy (EDS). Representative samples with different mineral compositions were selected for the X-ray diffraction (XRD) analysis, total organic content (TOC), porosity and permeability measurement, the low-pressure nitrogen adsorption analysis, and high-pressure mercury intrusion experiments (**Supplementary Tables S1, S2**).

3.1 Scanning Electron Microscopy Tests and Observation

Following optical microscope observation, thin section samples were coated with carbon to enhance conductivity and observed under a cold field scanning electron microscope. The device used was an FEI Quanta 650 FEG scanning electron microscope (SEM) equipped with an Oxford INCA Synergy EDS at the Key Laboratory of Orogenic Belts and Crustal Evolution, School of Earth and Space Sciences, Peking University. The acceleration voltage was 10–15 kV and the spot size was 5 μ m. Minerals were identified with EDS, and pore structures were observed in back-scattered electron (BSE) and secondary electron (SE) images. The BSE images of different pore types were selected to calculate pore areas and pore size distribution using ImageJ software.

3.2 X-Ray Diffraction (XRD)

XRD was applied to quantitatively determine the mineral components of both whole rocks and clay minerals. These tests were conducted at Beijing Beida Zhihui Microstructure Analysis and Testing Center Co., Ltd., using a Rigaku D/max-2500 diffractometer with a voltage of 48 kV and a current of 100 mA. For the whole rock analysis, each sample was crushed to 40-mesh and 5 g samples were analyzed. The 2θ scan range was set to 5–45°, with a scan speed of 2° per minute and sampling step width of 0.02°. For analysis of clay minerals, samples were first crushed to less than 1 mm, and carbonate and organic matter were removed. They were then dispersed using ultrasonic vibration, sucked into suspension, centrifuged, and dried to obtain powder before being placed in the diffractometer.

3.3 Total Organic Content (TOC)

The TOC content was obtained by using Leco CS230 carbon and sulfur analyzer at the China University of Petroleum (Beijing). Crushed all samples into powder under 200 mesh and then removed the inorganic carbon by HCl. To clean the HCl

before measurement, washed all samples with distilled water for about 24 h. Then dried samples were analyzed according to Chinese National Standard GB/T 19145-2003.

3.4 Porosity and Permeability Measurement

Porosity and permeability measurements were carried out at the China University of Petroleum (Beijing). The porosities and permeability were obtained by 2.5 cm * 2.5 cm * 5 cm-column samples. Measure the volume of samples by vernier caliper at first. The porosity was measured using a QKY-2 gas porosity tester. Put samples in the gripper and connect helium gas, then read after system pressure is stable. The permeability was obtained by PDP-200 pulse attenuation gas measuring ultra-low permeability tester, which can record data and calculate Kirschner permeability automatically.

3.5 Low-Pressure Nitrogen Adsorption (LPNA)

Low-temperature nitrogen adsorption was tested using a Micromeritics ASAP 2460 3.01 analyzer at Northeastern Petroleum University, China. Samples were pulverized to powder with sizes of 40–60 mesh and degassed to remove adsorbed water and other volatile substances. The equilibrium time interval between data points was set to 5 s. The specific surface areas were calculated using the BJH model. Pore volume (PV) and pore size distribution curves were deduced using the BET method.

3.6 Mercury Intrusion Porosimetry (MIP)

MIP was performed using a Micromeritics AutoPore IV 9520 mercury porosimeter at the China University of Geosciences (Wuhan). The instrument was operated at a maximum pressure of 60,000 Psia. 1 cm * 1 cm * 1 cm cubic samples were dried at 110°C and placed in a vacuum. Pore sizes were estimated from pressure data using the Washburn equation (Washburn, 1921).

4 RESULTS

4.1 Lithofacies of the Fengcheng Formation

The Fengcheng Formation in well My 1 is mainly composed of quartz, K-feldspar, plagioclase, dolomite, calcite, and pyrite. The main alkaline mineral is reedmergnerite, which is found in samples from the middle and lower intervals of the P_{1f_2} . The clay minerals are mostly illite, smectite, and illite/smectite mixed layer, with widely varying contents (2%–30%). Mudstones, siltstones, volcanic rocks, tuffs, and other lithologies were observed in the Fengcheng Formation. P_{1f_1} is dominated by tuffaceous sandstones, tuffaceous conglomerates, andesites, and basalts, with siliceous mudstones and dolomitic mudstones occurring in the upper interval. P_{1f_2} is predominantly composed of dolomitic mudstones, siliceous mudstones, and dolomites, with some mudstones and calcareous mudstones. Siliceous layers appear in the middle and lower intervals, with tuffaceous rocks only occurring in the top and bottom intervals.

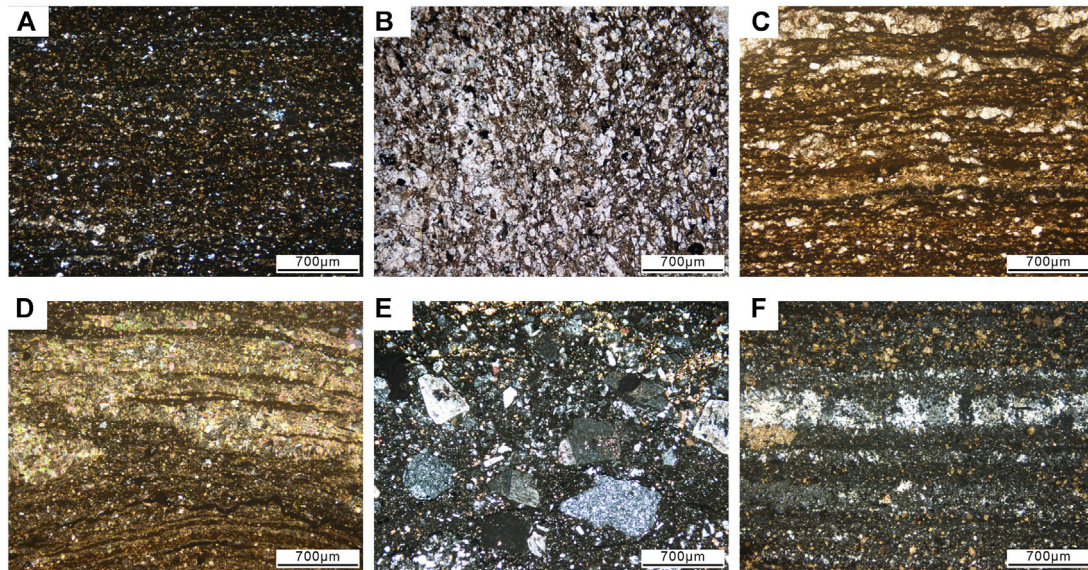


FIGURE 3 | Microscopic images of individual types of shales in the Fengcheng Formation from well My1. **(A)** Dolomitic mudstone, 4,592.08 m, under cross-polar light (XPL); **(B)** dolomitic mudstone, 4,749.03 m, under plane-polarized light (PPL); **(C)** argillaceous mudstone, 4,712.3 m, PPL; **(D)** calcareous mudstone, 4,596.51 m, XPL; **(E)** tuffaceous mudstone, 4,614.61 m, XPL; **(F)** siliceous mudstone, 4,814.6 m, XPL.

P_{1f3} is dominated by calcite mudstone with interbedded dolomitic mudstone and argillaceous mudstone. A small amount of tuffaceous mudstone appears at the bottom.

To better characterize the shale lithofacies of the Fengcheng Formation, shales were divided into five types based on their contents of dolomite, calcite, quartz, clay minerals, and tuffaceous materials, including dolomitic mudstone, siliceous mudstone, calcareous mudstone, tuffaceous mudstone, and argillaceous mudstone (**Figure 3**). They are characterized by a wide range of TOC values (**Supplementary Table S1**).

Dolomitic mudstone has 25%–50% dolomite with a TOC of 0.41–1.5. The dolomite particles are shown as fine, medium, and coarse crystals, which are mostly saccharoidal. Dolomite replacement is common, with the formation of ankerite zones. Bright rims and fogged cores are also observed under an optical microscope. Laminae are also common in the dolomitic mudstone. The calcite content of the calcareous mudstone is more than 25%, with laminae occurring and a relatively high content of dolomite. The content of quartz in the siliceous mudstone is over 25%, mostly subhedral or crypto-microcrystalline in texture, with small amounts of dolomite, calcite, and pyrite. The TOC of siliceous mudstones is 0.45–1.12. The tuffaceous mudstone is characterized by abundant tuffaceous debris and TOC is from 0.21 to 0.97. Compared with these four mudstone facies, the argillaceous mudstone has a relatively high clay content (>10%), and the contents of dolomite, calcite, and quartz are less than 25%. The TOC of argillaceous mudstone is 0.3–1.23. Lamination is relatively well developed in parts of the argillaceous mudstone that contain dark organic-rich bands. Since the content of reedmergerite in most of the samples is less than 10%, the

mudstones containing alkaline minerals are not listed individually.

The Fengcheng Formation contains massive, bedded, laminar, soft sedimentary deformation and other sedimentary structures. Laminae principally occur in the dolomitic mudstone, siliceous mudstone, and argillaceous mudstone. The proportions of laminae in P_{1f1} , P_{1f2} , and P_{1f3} are 7%, 35%, and 20%, respectively.

4.2 Pore Types

The Fengcheng Formation shale in well My1 has typical shale reservoir capabilities. The types of reservoir space include intergranular pores, intercrystalline pores, solution pores, and microfractures (**Figure 4**). The intercrystalline pores include interlayer fractures in clay minerals and intercrystalline pores in pyrites.

Intergranular pores are widespread, particularly in dolomitic mudstones, tuffaceous mudstone, and siltstones. They are mostly micron-scale pores supported by particles of brittle minerals such as calcite, dolomite, quartz, feldspar, and debris. The intergranular pores in **(Figure 4A)** are complex in shape, mostly silt-, triangle-, and band-shaped, or irregularly shaped. The intergranular pores are generally connected and their sizes are between 0.2 and 2 μm . Intercrystalline pores mostly occur in pyrite crystals and between clay mineral layers (**Figures 4B,C**). Clay minerals, in particular illite/smectite (I/S), have obvious slit-shaped pores between lamellae. Most of the intergranular pores in pyrites are angular in shape and generally 50–600 nm in size. The pores are mostly filled with organic matter or clay minerals.

Dissolution pores are also widely found, particularly in calcareous mudstone, tuffaceous mudstone, and siltstone. They are mostly intra- and inter-granular solution pores within and

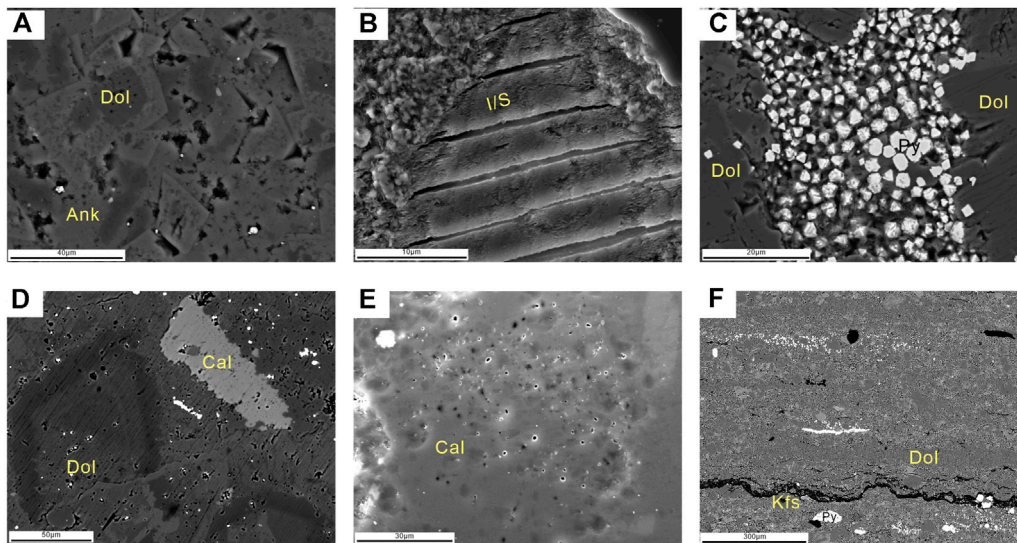
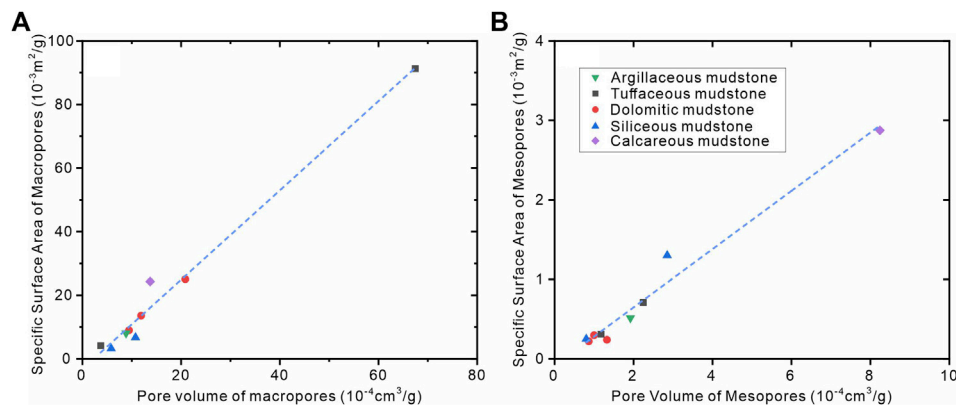
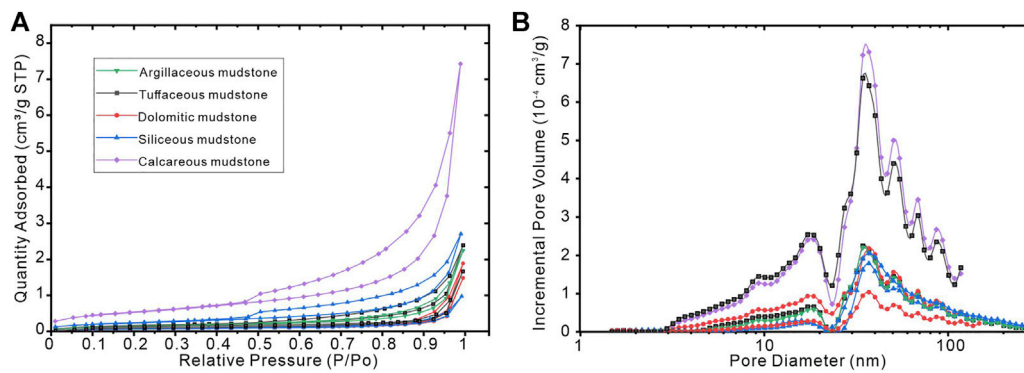
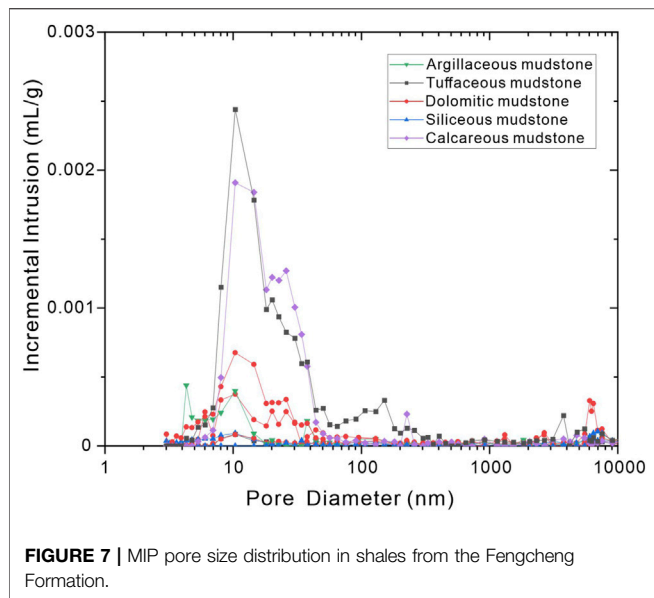


FIGURE 4 | SEM images of different types of pores in the Fengcheng Formation. **(A)** Intergranular pores and dissolution pores in dolomite and ankerite; **(B)** interlayer pores within I/S; **(C)** intercrystalline pores in pyrites; **(D,E)** dissolution pores within dolomite and calcite; **(F)** microfracture in the dolomitic mudstone. Ank = ankerite; Cal = calcite; Dol = dolomite; I/S = mixed-layer illite/smectite; Kfs = K-feldspar; Py = pyrite.





between particles of calcite, feldspar, and dolomite (Figures 4B,D,E). The surfaces of the dissolution pores are smooth and, overall, circular, elliptical, banded, or irregular in shape. The range of pore sizes is wide, from tens of nanometers to micrometers. Some of the dissolution pores are aggregated with good connectivity.

Microfractures also occur and cut minerals, or develop along the edges of mineral particles. Some are tectonic fractures, formed under tectonic stress, and some are bedding fractures formed between laminae under local stress. The fractures are usually tens of nanometers to several micrometers wide and have curved shapes and good extension (Figure 4F).

4.3 Pore Structure Distribution (PSD)

According to the IUPCA standard, pores with pore sizes of <2 nm, 2–50 nm, and >50 nm are defined as micropores, mesopores, and macropores, respectively. The Fengcheng Formation is proven to host shale oil, so only mesopores and macropores are considered in this study.

4.3.1 PSD Derived From LPNA

Low-pressure nitrogen adsorption (LPNA) tests obtained a pore distribution of 2–200 nm according to the BJH model. The nitrogen adsorption-desorption curves (Figure 5A) of the 16 samples represent type IV adsorption equilibrium isotherms within the IUPAC classification. In the low-specific pressure area ($p/p_0 < 0.45$), monolayer adsorption occurs, and adsorption and desorption are reversible. In the high-specific pressure area, adsorption and desorption are irreversible due to multilayer adsorption, forming hysteresis loops between the adsorption and desorption curves. In the mudstone samples from well My1, the type of hysteresis loop is mainly H_3 , often mixed with type H_4 and with some samples showing characteristics of type H_2 . Types H_3 and H_4 hysteresis loops

represent the parallel plate-shaped and slit-shaped pores, and type H_2 hysteresis loops represent the “ink bottle”-shaped pores.

The mesopore volume, obtained using the BJH model, ranges from 0.0002 to 0.0082 cm^3/g (average 0.0024 cm^3/g). The specific surface area of the mesopore, calculated by the BET model, ranges from 0.1249 to 2.8736 cm^2/g (average 0.8104 cm^2/g). The specific surface area of mesopore increases with increasing pore volume, showing a favorable correlation (Figure 6A).

The distribution of pore size and pore volume increments (Figure 5B) obtained in LPNA indicates that the maximum pore volume increment occurs when the pore sizes are 20–50 nm, followed by 10–20 nm. The pore volume increment should increase with the increase of pore size. This suggests that there are relatively few pores larger than 50 nm, but may also reflect the fact that LPNA does not work well with pores larger than 50 nm.

4.3.2 PSD Derived From MIP

Mercury injection tests were carried out on nine samples from well My1. Mercury injection saturation was low, mostly between 30% and 40%. The mercury injection curves obtained can be divided into types A, B, and C. The horizontal section of the type A mercury injection curve is long and gentle, and the mercury injection amount is 35–40%. The horizontal section of mercury injection curves of type B occurs when mercury saturation is about 10%, then slowly rises. The mercury injection amount is 35–40%. The mercury injection curve of type C has almost no horizontal section, and the amount of mercury injection is 30–40%.

The pore diameters obtained by MIP are ranging from 2 nm to 10 μm . The distribution of pore diameter and pore volume increments curve (Figure 7) obtained in MIP is multimodal. The maximum pore volume increment occurs when the pore diameters are 7–40 nm, following at 7–10 μm .

The macropore volume, obtained by MIP, ranges from 0.00037 to 0.0067 cm^3/g (average 0.0017 cm^3/g). The specific surface area of macropores by MIP ranges from 0.0032 to 0.0913 cm^2/g (average 0.0206 cm^2/g). The specific surface area of the macropore increases with increasing pore volume, also showing a favorable correlation (Figure 6B).

5 DISCUSSION

5.1 Pore Structures of Different Shale Lithofacies

Lithofacies refers to petrological characteristics and mineralogical compositions and can show different pore structures. Therefore, pore development and structures would vary with shale lithofacies (Loucks and Ruppel, 2007; Xu et al., 2020; Wang et al., 2022). Comprehensive studies of marine, transition, and continental shale lithofacies have been conducted without reaching any standard (e.g., Gao et al., 2018; Yang et al., 2018; Xue et al., 2020). We here introduced shale lithofacies based mainly on mineral composition. Five lithofacies have been identified: dolomitic mudstone, calcareous mudstone, siliceous mudstone, tuffaceous mudstone, and argillaceous mudstone. The TOC values are not controlled by any specific lithofacies.

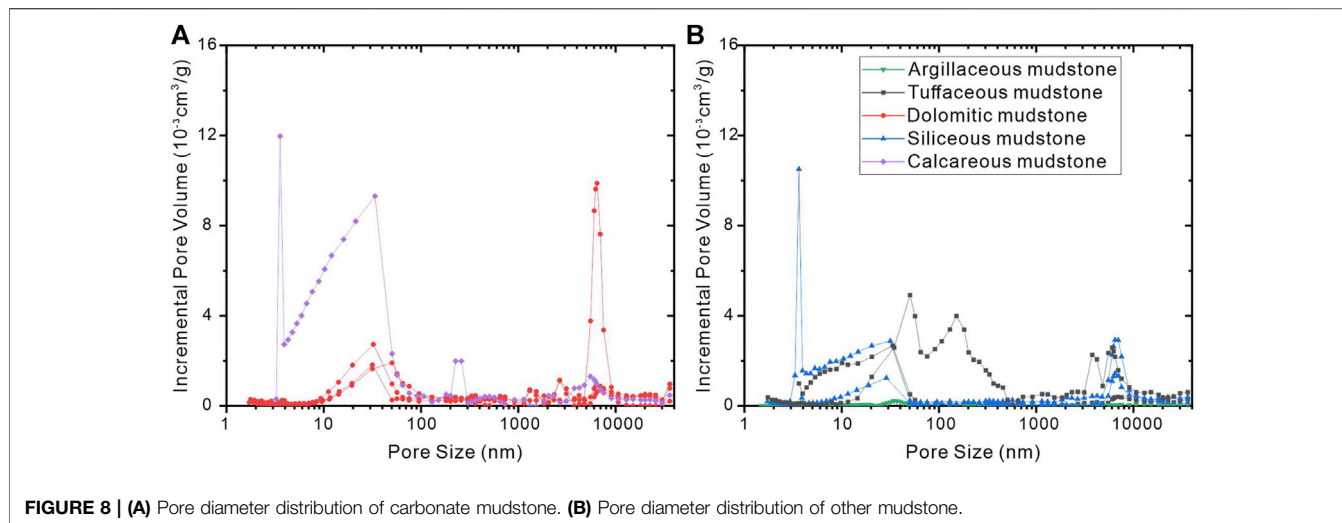


FIGURE 8 | (A) Pore diameter distribution of carbonate mudstone. **(B)** Pore diameter distribution of other mudstone.

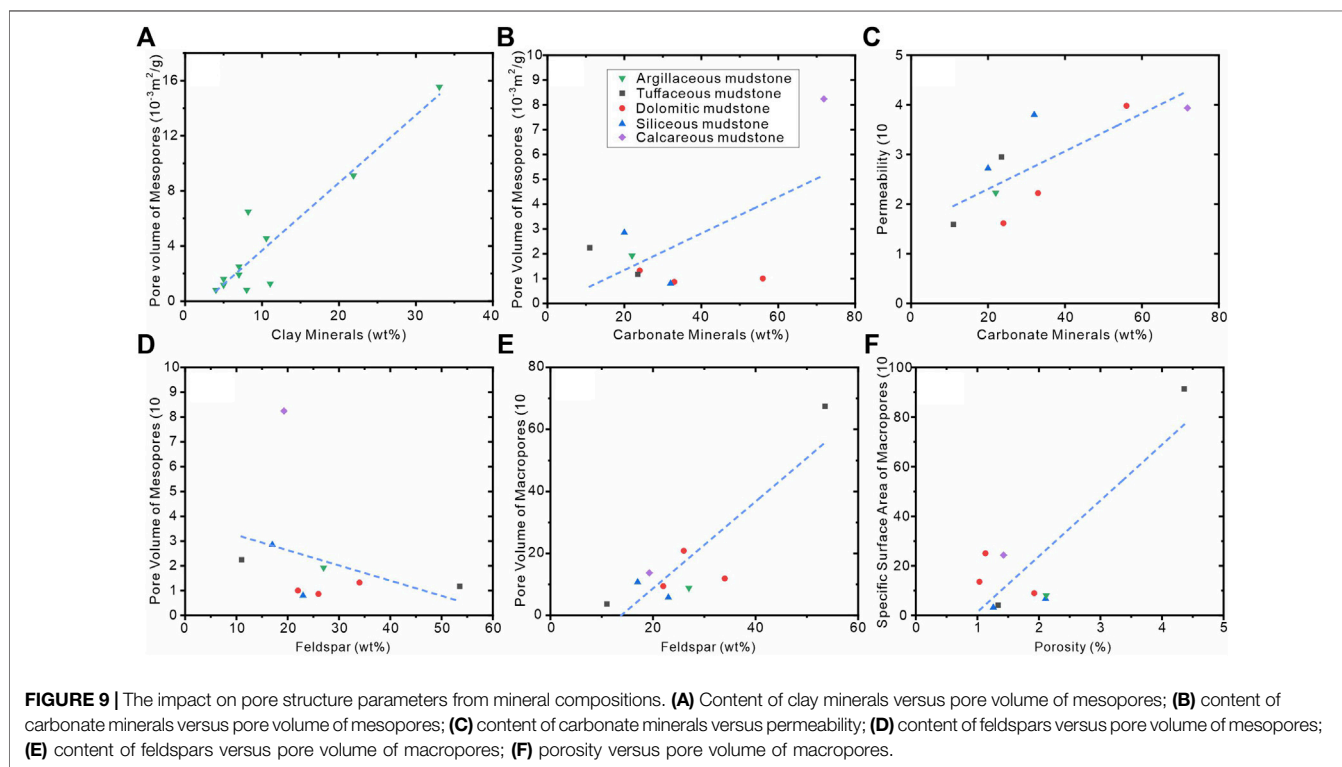


FIGURE 9 | The impact on pore structure parameters from mineral compositions. **(A)** Content of clay minerals versus pore volume of mesopores; **(B)** content of carbonate minerals versus pore volume of mesopores; **(C)** content of carbonate minerals versus permeability; **(D)** content of feldspars versus pore volume of mesopores; **(E)** content of feldspars versus pore volume of macropores; **(F)** porosity versus pore volume of macropores.

The single method with its limitations cannot characterize the full-scale structure due to the wide ranges of shale pore distribution (Zhao et al., 2022; Daigle et al., 2015). The whole pore aperture was quantitatively achieved with the combination of LPNA and MIP results (Figure 8). Based on the limitations of the two methods in the test range (Xiong et al., 2016; Zheng et al., 2022), the LPNA results were used for <50 nm and the MIP results were used for >50 nm. The curves of LPNA and MIP combination results show a wide range of pore diameter from 2 nm to micron-scale with the multimodal distribution. The curves of pore

volume versus pore diameter can be divided into three segments, including pore diameter <50 nm, 50 nm–4 μm, and >4 μm (Figure 4). There are three high peaks and two relatively lower peaks in the pore diameter intervals of 3 nm, 20–40 nm, and 7–10 μm. The distribution peak at 3 nm is generally considered to be a false peak caused by testing technology limitations. The distribution peak at 20–40 nm and 7–10 μm will be discussed in detail in the following chapters.

The pore structures of five different lithofacies have distinguishable characteristics. The tuffaceous mudstones

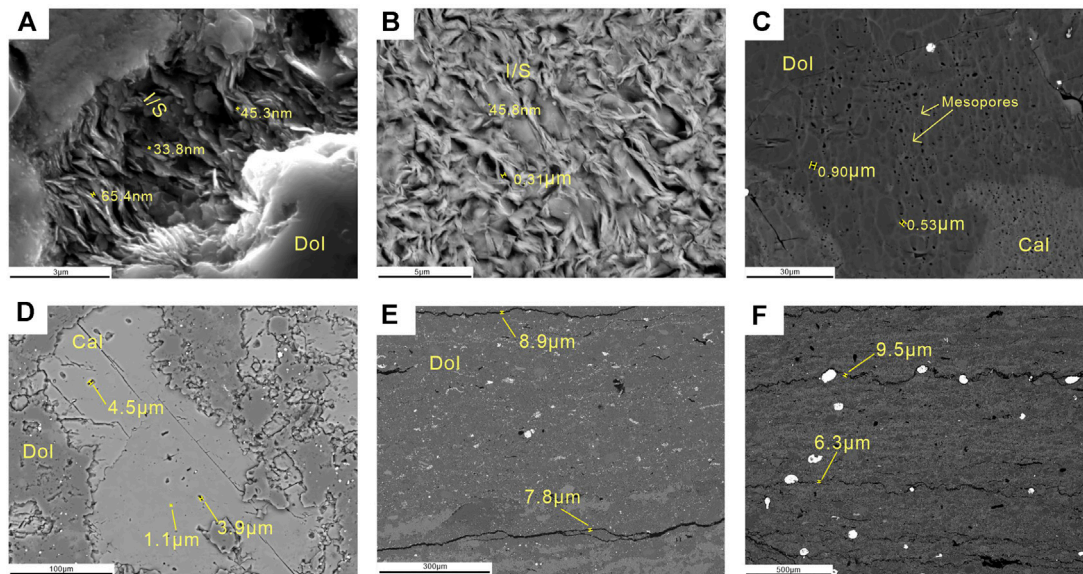


FIGURE 10 | SEM photographs of samples. **(A,B)** Intercrystalline pores of clay minerals; **(C,D)** dissolution pores of carbonate minerals; **(E,F)** microfractures between laminae. Cal: calcite; Dol: dolomite; I/S: mixed-layer illite/smectite.

develop 20–200 nm mesopores and macropores and have a peak of 4–7 μm macropores. Pore diameters of dolomitic mudstones have two peaks, at 10–60 nm and 4–10 μm, respectively, the latter peak is higher than the former. Calcareous mudstone mainly develops the mesopores, with the highest peak in 4–40 nm, following a lower peak for 200–300 nm, and the lowest peak in 3–10 μm. Siliceous mudstones show peaks of pore diameter within 10–50 nm and 5–9 μm, and low pore volume developed within 50 nm–5 μm. Macropores in argillaceous mudstone are poorly developed and there is only one peak at 20–50 nm. In terms of pore structures and distributions, our lithofacies classification based on mineral composition is thus practical.

5.2 Mineral Composition Influences on Pore Structure

5.2.1 Effect of Clay Minerals

Clay minerals in the Fengcheng Formation of well My1 are mainly smectite, I/S, and illite. The content of clay minerals is relatively low, ranging from 2% to 30%, mainly 4%–8%, higher in argillaceous mudstones. Clay components in shales are closely related to the mesopores whose pore diameter ranges from 2 to 17 nm. Particularly, the existence of I/S may be correlated with fine mesopores (Kuila and Prasad, 2013).

The N_2 adsorption and desorption curves of samples separate and form hysteresis loops. The hysteresis loops are H3 and H4 types (Figure 5), which indicates the existence of parallel plate or wedge-shaped pores (Sing, 1985; Tang et al., 2019). The intercrystalline pores and interlayer fractures of clay minerals are widely developed in the reservoir of well My1, which can be observed under SEM (Figures 10A,B). The pore diameters of intergranular pores associated with clay minerals are between

20–40 nm and often appear as parallel plate shapes. The H3 type hysteresis is thus considered to be related to intergranular pores of clay minerals.

In order to better explore the relationship between clay minerals and mesoporous pores, nine argillaceous mudstones from well My 1 were explored by obtaining the content of clay minerals by XRD and the cumulative pores volume of mesopores by LNPA. There is a positive correlation (Figure 9A) between mesopore volumes and clay minerals content, suggesting that clay minerals have strong effects on mesopore structure. Furthermore, the pore volume of mesopores shows a positive correlation with mixed-layer illite/smectite (I/S) and smectite (Supplementary Figure S1). It is consistent with the 20–50 nm peak of all kinds of mudstones in the pore size distribution curve, which should be the contributions of intergranular pores of clay minerals. Overall, clay minerals, especially I/S and smectite, are closely correlated with micropore structures.

5.2.2 Effect of Carbonate Minerals

Dolomite and calcite are the main carbonate minerals widely developed in the Fengcheng Formation of Mahu Sag. The samples with high carbonate mineral contents show stronger dissolution, especially for calcareous mudstone and dolomitic mudstone (Figures 10C,D). The early calcite filling or cement may occupy pores or block pore throats, but favorable reservoirs could be developed with strong dissolution in later periods (Lu et al., 2021). Calcite and dolomite dissolved more easily than K-feldspar and plagioclase and the calcite dissolution usually occurred earlier than the dolomite dissolution (Chen et al., 2020).

The XRD results show that the carbonate composition of samples can reach 20%–65%. Abundant dissolution pores on the surface of carbonate minerals have a wide range of pore size

distribution, ranging from tens of nanometers to several microns, but nanoscale pores dominate. These pore diameters are consistent with macropore peaks of dolomitic mudstone and calcareous mudstone (DC). There is a positive correlation between carbonate minerals and the accumulated pore volume of mesopores (**Figure 9B**), indicating that carbonate minerals also control the development of mesopores, and this favorable trend largely comes from the development of dissolution pores in carbonate minerals. Moreover, permeability increases with the increase of carbonate mineral content (**Figure 9C**), which indicates that carbonate minerals have an important effect on permeability. The dissolution pores of carbonate minerals appear to improve the connectivity of the reservoir.

5.2.3 Effect of Feldspars

The content of feldspar has a negative correlation with the pore volume of mesopores (**Figure 9D**), indicating the negative effect of feldspar on mesopore development. However, the feldspar is positively correlated with macropore volume (**Figure 9E**), suggesting feldspars contribute to a large number of macropores. The dissolution pores in feldspars are observed to be developed in all mudstones, especially in tuffaceous mudstone.

Because the content of feldspar in tuffaceous mudstone is high and feldspar is easily dissolved, the main storage spaces of tuffaceous mudstone are secondary pores formed by feldspar dissolution (Li et al., 2022). A large number of macropores with a diameter greater than 50 nm are shown in tuffaceous mudstones, mainly associated with feldspars. Therefore, the content of feldspar is reasonable to explain well-developed macropores in tuffaceous mudstones.

5.3 Effect of Laminae Structure on Pore Structure

The lamina structure is of great significance for reservoir quality and oil-bearing potential in shales (Liang et al., 2018; Wang et al., 2021; Shi et al., 2022). Many laminae are developed in the Fengcheng Formation, including organic-rich dark layers + carbonate mineral layers and clay mineral-rich argillaceous layers + carbonate mineral layers (Wang et al., 2021). These laminae were generally developed in dolomitic mudstones, and microfractures were preferentially developed between layers with micron-scale widths (**Figures 10E,F**). These microfractures are considered to be formed by mineral shrinkages or decompression from overburden (Chalmers and Bustin, 2012).

Despite some microfractures filled with clay minerals, most laminated samples have relatively high porosity and permeability, and the pore volume distribution curve shows that the major contributions to pore structures come from macropores, which correspond to the diameters of microfractures between laminae.

5.4 Implication for High-Quality Shale Reservoir

Lacustrine shale oil is a key strategic supplement to the sustainability of China's oil industry (Wang et al., 2022). The Fengcheng Formation is a set of high-quality source rocks of Mahu

Sag, Junggar Basin (Tang et al., 2021). We take well My 1 as a research object and make lithofacies classification of alkaline lacustrine shales. The mudstones are divided into dolomitic mudstone, siliceous mudstone, calcareous mudstone, tuffaceous mudstone, and argillaceous mudstone based on rock composition. The dolomitic mudstone is the dominant lithofacies in well My 1. There are distinguishable curves of pore structure distribution of different shale lithofacies, indicating different influencing factors for these different lithofacies.

The Fengcheng Formation in well My 1 has low porosity and ultra-low-permeability, as other shales. Poor correlation between porosity and permeability indicates that pore structures should play a key role in the permeability besides porosity (Wang et al., 2018). There is a positive correlation between the porosity and the pore volume of macropores (**Figure 9F**), indicating that macropores contribute more to the overall porosity of samples. All five types of mudstones have a peak in the range of a mesoporous scale in pore structure distribution, which is mainly provided by clay minerals. Dolomitic mudstone is dominated by mesopores because of dissolution pores, and microfractures associated with laminae contribute to macropores volume for dolomitic mudstone. The macropores of siliceous mudstone are mainly intergranular pores between quartz (Cao et al., 2022) because the rigid quartz can protect the pore network from compaction effects (Tang et al., 2019). There are a lot of mesopores in argillaceous mudstone, mainly related to clay minerals, and the proportion of macropores is low. The macropores in calcareous mudstones are provided by the dissolution of calcite. The tuffaceous mudstone has plenty of macropores because of the dissolution of feldspars and tuffaceous mudstone is also favorable lithofacies. Therefore, laminated dolomitic mudstones and tuffaceous mudstones are proposed to be high-quality shale lithofacies with great exploration potential in the Fengcheng Formation from well My1.

The well My 1 is in the slope zones in the Mahu Sag (Tang et al., 2019), with few alkaline minerals except small amounts of reedmergnerite, so our study lack discussion on the relationship between alkaline minerals and reservoir development. In the future, with the development of exploration technology and more drilling cores, further systematic research on alkaline mineral-bearing mudstones needs to be done in order to explore what controls alkaline lacustrine shales in terms of reservoir evolution.

6 CONCLUSION

- 1) The Fengcheng Formation is considered to be alkaline lacustrine shale with high potential in shale oil in the Mahu Sag, Junggar Basin. Shales in well My 1 are divided into five types: dolomitic mudstone, calcareous mudstone, siliceous mudstone, tuffaceous mudstone, and argillaceous mudstone mainly based on mineral composition.
- 2) There are intragranular and inter-crystalline pores associated with clays and pyrites, dissolution pores, and microfractures commonly in these five types of mudstones. The overall pore structure can be divided into three segments, including <50 nm, 50 nm-4 μm , and >4 μm .

- 3) Each type of shale lithofacies has its pore structure. Clay minerals provide mainly mesopores in argillaceous mudstones. The dissolution of carbonate minerals and feldspars are significant for macropores which develop in dolomitic mudstones and tuffaceous mudstones, respectively. Micro-scale microfractures associated with laminae dominate in dolomitic mudstones.
- 4) The dolomitic mudstones and tuffaceous mudstones have better resource potential and should be given more attention in the future in Mahu Sag. More investigations on alkaline mineral-bearing mudstones are in need in the future.

DATA AVAILABILITY STATEMENT

The datasets presented in this study can be found in online repositories. The names of the repository/repositories and accession number(s) can be found in the article/**Supplementary Material**.

AUTHOR CONTRIBUTIONS

YT: conceptualization, resources. WH: methodology. MZ: methodology. QC: methodology. ZJ: supervision. JL:

REFERENCES

- Barth-Naftilan, E., Aloysius, N., and Saiers, J. E. (2015). Spatial and Temporal Trends in Freshwater Appropriation for Natural Gas Development in Pennsylvania's Marcellus Shale Play. *Geophys. Res. Lett.* 42 (15), 6348–6356. doi:10.1002/2015GL065240
- Cao, J., Lei, D. W., Li, Y. W., Tang, Y., AbulimitChang, Q. S., et al. (2015). Ancient High-Quality Alkaline Lacustrine Source Rocks Discovered in the Lower Permian Fengcheng Formation, Junggar Basin. *Acta Pet. Sin.* 36 (07), 781–790. (in Chinese with English Abstract). doi:10.7623/syxb201507002
- Cao, J., Xia, L., Wang, T., Zhi, D., Tang, Y., and Li, W. (2020). An Alkaline Lake in the Late Paleozoic Ice Age (LPIA): A Review and New Insights into Paleoenvironment and Petroleum Geology. *Earth-Sci. Rev.* 202, 103091. doi:10.1016/j.earscirev.2020.103091
- Cao, T., Liu, H., Pan, A., Fu, Y., Deng, M., Cao, Q., et al. (2022). Pore Evolution in Siliceous Shales and its Influence on Shale Gas-Bearing Capacity in Eastern Sichuan-Western Hubei, China. *J. Pet. Sci. Eng.* 208, 109597. doi:10.1016/j.petrol.2021.109597
- Chalmers, G. R. L., and Bustin, R. M. (2012). Geological Evaluation of Halfway-Doig-Montney Hybrid Gas Shale-Tight Gas Reservoir, Northeastern British Columbia. *Mar. Pet. Geol.* 38 (1), 53–72. doi:10.1016/j.marpetgeo.2012.08.004
- Chen, L., Jiang, Z., Liu, Q., Jiang, S., Liu, K., Tan, J., et al. (2019). Mechanism of Shale Gas Occurrence: Insights from Comparative Study on Pore Structures of Marine and Lacustrine Shales. *Mar. Pet. Geol.* 104, 200–216. doi:10.1016/j.marpetgeo.2019.03.027
- Chen, X., Qu, X. Y., Xu, S. Y., Wang, W. M., Li, S. M., He, H., et al. (2020). Dissolution Pores in Shale and Their Influence on Reservoir Quality in Damintun Depression, Bohai Bay Basin, East China: Insights from SEM Images, N₂ Adsorption and Fluid-Rock Interaction Experiments. *Mar. Pet. Geol.* 117, 104394. doi:10.1016/j.marpetgeo.2020.104394
- Daigle, H., and Johnson, A. (2016). Combining Mercury Intrusion and Nuclear Magnetic Resonance Measurements Using Percolation Theory. *Transp. Porous Med.* 111 (3), 669–679. doi:10.1007/s11242-015-0619-1
- Gao, F., Song, Y., Li, Z., Xiong, F., Chen, L., Zhang, Y., et al. (2018). Lithofacies and Reservoir Characteristics of the Lower Cretaceous Continental Shahezi Shale in the Changling Fault Depression of Songliao Basin, NE China. *Mar. Pet. Geol.* 98, 401–421. doi:10.1016/j.marpetgeo.2018.08.035
- He, D. F., Zhang, L., Wu, S. T., Li, D., and Zhen, Y. (2018). Tectonic Evolution Stages and Features of the Junggar Basin. *Oil Gas Geol.* 39 (05), 845–861. (in Chinese with English Abstract). doi:10.11743/ogg20180501
- Hu, S. Y., Bai, B., Tao, S. Z., Bian, C. S., Zhang, T. S., Chen, Y. Y., et al. (2022). Heterogeneous Geological Conditions and Differential Enrichment of Medium and High Maturity Continental Shale Oil in China. *Pet. Explor. Dev.* 49 (02), 224–237. (in Chinese with English Abstract). doi:10.1016/s1876-3804(22)60022-3
- Jin, Z. J., Zhu, R. K., Liang, X. P., and Shen, Y. Q. (2021). Several Issues Worthy of Attention in Current Lacustrine Shale Oil Exploration and Development. *Pet. Explor. Dev.* 48 (06), 1276–1287. (in Chinese with English Abstract). doi:10.1016/s1876-3804(21)60303-8
- Kuila, U., and Prasad, M. (2013). Specific Surface Area and Pore-Size Distribution in Clays and Shales. *Geophys. Prospect.* 61 (2), 341–362. doi:10.1111/1365-2478.12028
- Li, M. W., Ma, X. X., Jiang, Q. G., Li, Z. M., Pang, X. Q., Zhang, C. T., et al. (2019). Enlightenment from Formation Conditions and Enrichment Characteristics of Marine Shale Oil in North America. *Pet. Geol. Recovery Effic.* 26 (01), 13–28. (in Chinese with English Abstract). doi:10.13673/j.cnki.cn37-1359/te.2019.01.002
- Li, W., Zhang, Y. Y., Ni, M. J., and Tang, W. B. (2020). Genesis of Alkaline Lacustrine Deposits in the Lower Permian Fengcheng Formation of the Mahu Sag, Northwestern Junggar Basin: Insights from a Comparison with the Worldwide Alkaline Lacustrine Deposits. *Acta Geol. Sin.* 94 (06), 1839–1852. (in Chinese with English Abstract). doi:10.19762/j.cnki.dizhixuebao.2020087
- Li, Q., Lu, H., Li, J., Wu, S., Wu, Y., Wen, L., et al. (2022). Characteristics and Formation Mechanism of the Tight Tuff Reservoirs of the Upper Triassic Chang 7 Member in the Southern Ordos Basin, China. *Mar. Pet. Geol.* 139, 105625. doi:10.1016/j.marpetgeo.2022.105625
- Liang, C., Cao, Y., Liu, K., Jiang, Z., Wu, J., and Hao, F. (2018). Diagenetic Variation at the Lamina Scale in Lacustrine Organic-Rich Shales: Implications for Hydrocarbon Migration and Accumulation. *Geochim. Cosmochim. Acta* 229, 112–128. doi:10.1016/j.gca.2018.03.017

writing—original draft, data processing. YZ: writing—review and editing.

FUNDING

This research was supported by the Natural Science Foundation of China (NSFC) Project given to Prof. Zhaojie Guo (No. 42090021).

ACKNOWLEDGMENTS

We would like to acknowledge PetroChina Xinjiang Oilfield Company for their assistance. We are grateful to Dr. Dongdong Li and two reviewers for the constructive reviews of the manuscript.

SUPPLEMENTARY MATERIAL

The Supplementary Material for this article can be found online at: <https://www.frontiersin.org/articles/10.3389/feart.2022.930890/full#supplementary-material>

- Loucks, R. G., and Ruppel, S. C. (2007). Mississippian Barnett Shale: Lithofacies and Depositional Setting of a Deep-Water Shale-Gas Succession in the Fort Worth Basin, Texas. *Bulletin* 91 (4), 579–601. doi:10.1306/11020606059
- Lu, X., Cao, Y. C., Bian, B. L., Liu, H. L., Wang, X. X., Zhao, Y. W., et al. (2021). Genesis of Calcite Vein in Basalt and its Effect on Reservoir Quality: A Case Study of the Carboniferous in the East Slope of Mahu Sag, Junggar Basin, NW China. *Pet. Explor. Dev.* 48 (4), 864–876. doi:10.1016/S1876-3804(21)60072-1
- Ma, Z. J., Qu, G. S., and Chen, X. F. (2008). The Deep-Shallow Structures and Oil-Gas Distribution in Junggar Basin. *Xinjiang Pet. Geol.* 29 (04), 13–16. (in Chinese with English Abstract).
- Shi, J., Jin, Z., Liu, Q., Zhang, T., Fan, T., and Gao, Z. (2022). Laminar Characteristics of Lacustrine Organic-Rich Shales and Their Significance for Shale Reservoir Formation: A Case Study of the Paleogene Shales in the Dongying Sag, Bohai Bay Basin, China. *J. Asian Earth Sci.* 223, 104976. doi:10.1016/j.jseae.2021.104976
- Sing, K. S. W. (1985). Reporting Physisorption Data for Gas/solid Systems with Special Reference to the Determination of Surface Area and Porosity (Recommendations 1984). *Pure. Appl. Chem.* 57 (4), 603–619. doi:10.1351/pac198557040603
- Tang, L., Song, Y., Jiang, Z., Jiang, S., and Li, Q. (2019). Pore Structure and Fractal Characteristics of Distinct Thermally Mature Shales. *Energy Fuels*. 33 (6), 5116–5128. doi:10.1021/acs.energyfuels.9b00885
- Tang, Y., Cao, J., He, W.-J., Guo, X.-G., Zhao, K.-B., and Li, W.-W. (2021). Discovery of Shale Oil in Alkaline Lacustrine Basins: The Late Paleozoic Fengcheng Formation, Mahu Sag, Junggar Basin, China. *Pet. Sci.* 18 (5), 1281–1293. doi:10.1016/j.petsci.2021.04.001
- Wang, T., Cao, J., Jin, J., Xia, L., Xiang, B., Ma, W., et al. (2021). Spatiotemporal Evolution of a Late Paleozoic Alkaline Lake in the Junggar Basin, China. *Mar. Pet. Geol.* 124, 104799. doi:10.1016/j.marpetgeo.2020.104799
- Wang, Z., Pan, M., Shi, Y., Liu, L., Xiong, F., and Qin, Z. (2018). Fractal Analysis of Donghetang Sandstones Using NMR Measurements. *Energy Fuels*. 32 (3), 2973–2982. doi:10.1021/acs.energyfuels.7b03463
- Wang, T., Cao, J., Carroll, Zhi, A. R. D. M., Zhi, D., Tang, Y., Wang, X., et al. (2020). Oldest Preserved Sodium Carbonate Evaporite: Late Paleozoic Fengcheng Formation, Junggar Basin, NW China. *Geol. Soc. Am. Bull.* 133 (7–8), 1465–1482. doi:10.1130/B35727.1
- Washburn, E. W. (1921). The Dynamics of Capillary Flow. *Phys. Rev.* 17 (3), 273–283. doi:10.1103/PhysRev.17.273
- Wang, E., Guo, T., Li, M., Li, C., Dong, X., Zhang, N., et al. (2022). Exploration Potential of Different Lithofacies of Deep Marine Shale Gas Systems: Insight into Organic Matter Accumulation and Pore Formation Mechanisms. *J. Nat. Gas Sci. Eng.* 102, 104563. doi:10.1016/j.jngse.2022.104563
- Wang, S., Wang, G., Huang, L., Song, L., Zhang, Y., Li, D., et al. (2021). Logging Evaluation of Lamina Structure and Reservoir Quality in Shale Oil Reservoir of Fengcheng Formation in Mahu Sag, China. *Mar. Pet. Geol.* 133, 105299. doi:10.1016/j.marpetgeo.2021.105299
- Wang, X., Zhang, G., Tang, W., Wang, D., Wang, K., Liu, J., et al. (2022). A Review of Commercial Development of Continental Shale Oil in China. *Energy Geosci.* 3 (3), 282–289. doi:10.1016/j.engeos.2022.03.006
- Xiong, Q., Baychev, T. G., and Jivkov, A. P. (2016). Review of Pore Network Modelling of Porous Media: Experimental Characterisations, Network Constructions and Applications to Reactive Transport. *J. Contam. Hydrol.* 192, 101–117. doi:10.1016/j.jconhyd.2016.07.002
- Xu, S., Gou, Q., Hao, F., Zhang, B., Shu, Z., Lu, Y., et al. (2020). Shale Pore Structure Characteristics of the High and Low Productivity Wells, Jiaoshiba Shale Gas Field, Sichuan Basin, China: Dominated by Lithofacies or Preservation Condition? *Mar. Pet. Geol.* 114, 104211. doi:10.1016/j.marpetgeo.2019.104211
- Xue, C., Wu, J., Qiu, L., Zhong, J., Zhang, S., Zhang, B., et al. (2020). Lithofacies Classification and its Controls on the Pore Structure Distribution in Permian Transitional Shale in the Northeastern Ordos Basin, China. *J. Pet. Sci. Eng.* 195, 107657. doi:10.1016/j.petrol.2020.107657
- Yang, W., Zuo, R., Jiang, Z., Chen, D., Song, Y., Luo, Q., et al. (2018). Effect of Lithofacies on Pore Structure and New Insights into Pore-Preserving Mechanisms of the Over-mature Qiongzhusi Marine Shales in Lower Cambrian of the Southern Sichuan Basin, China. *Mar. Pet. Geol.* 98, 746–762. doi:10.1016/j.marpetgeo.2018.09.020
- Zhao, R., Xue, H., Lu, S., Li, J., Tian, S., Wang, M., et al. (2022). Multi-scale Pore Structure Characterization of Lacustrine Shale and its Coupling Relationship with Material Composition: An Integrated Study of Multiple Experiments. *Mar. Pet. Geol.* 140, 105648. doi:10.1016/j.marpetgeo.2022.105648
- Zheng, H., Yang, F., Guo, Q., Pan, S., Jiang, S., and Wang, H. (2022). Multi-scale Pore Structure, Pore Network and Pore Connectivity of Tight Shale Oil Reservoir from Triassic Yanchang Formation, Ordos Basin. *J. Pet. Sci. Eng.* 212, 110283. doi:10.1016/j.petrol.2022.110283
- Zhi, D. M., Tang, Y., Zheng, M. L., Xu, Y., Cao, J., Ding, J., et al. (2019). Geological Characteristics and Accumulation Controlling Factors of Shale Reservoirs in Fengcheng Formation, Mahu Sag, Junggar Basin. *China Pet. Explor.* 24 (05), 615–623. (in Chinese with English Abstract). doi:10.3969/j.issn.1672-7703.2019.05.008
- Zhi, D. M., Tang, Y., He, W. J., Guo, X. G., Zheng, M. L., and Huang, L. L. (2021). Orderly Coexistence and Accumulation Models of Conventional and Unconventional Hydrocarbons in Lower Permian Fengcheng Formation, Mahu Sag, Junggar Basin. *Pet. Explor. Dev.* 48 (01), 38–51. (in Chinese with English Abstract). doi:10.1016/s1876-3804(21)60004-6
- Zou, C. N., Zhang, G. S., Yang, Z., Tao, S. Z., Hou, L. H., Zhu, R. K., et al. (2013). Geological Concepts, Characteristics, Resource Potential and Key Techniques of Unconventional Hydrocarbon: On Unconventional Petroleum Geology. *Pet. Explor. Dev.* 40 (04), 385–399+454. (in Chinese with English Abstract). doi:10.1016/s1876-3804(13)60053-1

Conflict of Interest: Authors YT, WH, MZ, and QC were employed by the company PetroChina Xinjiang Oilfield Company.

The remaining authors declare that the research was conducted in the absence of any commercial or financial relationships that could be construed as a potential conflict of interest.

Publisher's Note: All claims expressed in this article are solely those of the authors and do not necessarily represent those of their affiliated organizations, or those of the publisher, the editors, and the reviewers. Any product that may be evaluated in this article, or claim that may be made by its manufacturer, is not guaranteed or endorsed by the publisher.

Copyright © 2022 Tang, He, Zheng, Chang, Jin, Li and Zhang. This is an open-access article distributed under the terms of the Creative Commons Attribution License (CC BY). The use, distribution or reproduction in other forums is permitted, provided the original author(s) and the copyright owner(s) are credited and that the original publication in this journal is cited, in accordance with accepted academic practice. No use, distribution or reproduction is permitted which does not comply with these terms.